PROCEEDINGS, 45th Workshop on Geothermal Reservoir Engineering
Stanford University, Stanford, California, February 10-12, 2020
SGP-TR-216

Distributed Acoustic Sensing Monitoring at the First EGS Collab Testbeds

David Li[1], Lianjie Huang[1], Benxin Chi[1], Jonathan Ajo-Franklin[2,3], Verónica Rodríguez Tribaldos[2], Martin Schoenball[2], Timothy Kneafsey[2] , and the EGS Collab Team[*]

[1]Los Alamos National Laboratory, Geophysics Group, MS D452, Los Alamos, NM 87545, USA

[2]Lawrence Berkeley National Laboratory, 1 Cyclotron Road, Berkeley, CA 94720, USA

[3]Rice University, 6100 Main Street, Houston, TX 77005, USA

davidzli@lanl.gov; ljh@lanl.gov;

Keywords: Distributed Acoustic Sensing, Enhanced Geothermal Systems, Stimulation, EGS Collab, Fracture, Monitoring

ABSTRACT

Distributed Acoustic Sensing (DAS) employs a fiber-optic cable as a seismic sensor. In a DAS survey, a fiber optic cable is either cemented in a borehole or buried at the surface of the survey area. An interrogator unit is attached to one end of the cable and sends laser pulses down the length of the fiber to measure deformations in the fiber caused by passing seismic waves. The EGS Collab project is to study the fracture stimulation and monitoring for enhanced geothermal systems (EGS). The first testbed is located at 4850 ft. beneath the surface at the Sanford Underground Research Facility in South Dakota. The testbed consists of a stimulation well, a production well, and six monitoring wells drilled around a fracture stimulation zone. A length of optic fiber was deployed along the monitoring wells to continuously monitor during hydraulic stimulations. The gauge length for data collection was set to 10 m. We analyze the DAS data and compare the signal changes before, during, and after the hydraulic stimulations. We then compare the time-lapse monitoring results obtained from DAS data with results obtained from continuous active-source seismic monitoring (CASSM) data to study the feasibility of DAS for monitoring hydraulic fracturing in EGS reservoirs. In our preliminary results, we do not observe any scattered signal on the DAS data which may be caused by the large (10 m) gauge length used during data acquisition.

1. INTRODUCTION

Distributed Acoustic Sensing is a technology that employs an optical fiber cable as a sensor to measure strain-rate changes continuously in both space and time. In a DAS survey, a length of optical fiber cable is deployed either in boreholes or buried at the surface of an acquisition site. One end of the fiber is attached to an interrogator box that sends laser pulses down the length of the fiber. When the laser pulse encounters imperfections in the material of the fiber, some of the light are scattered and reflected back towards the integrator box that records its phase in a reference loop. During data acquisition/monitoring, a seismic wave passes through the fiber and causes the fiber to either extend or contract. This deformation causes a phase delay in the backscattered light. The interrogator box measures and converts this phase change to an average strain-rate (or strain) measurement over a finite length of fiber (gauge length). (Mestayer et al. 2011; Molenaar et al. 2012; Daley et al. 2016; ; Poletto et al 2016; Mateeva et al. 2014; Karrenbach et al. 2019; Jousset et al. 2019).

In real world applications, DAS has been deployed for both earthquake monitoring (Martin et al. 2016; Ajo-Franklin et al. 2018; Zhu and Strensrud. 2019), reservoir monitoring (Mateeva et al. 2013; Karrenbach et al. 2019), and for seismic exploration (Daley et al. 2016; Jousset et al. 2018). There are many advantages in collecting seismic data using DAS over conventional geophones. For one, DAS data are usually collected using standard telecommunication optic fiber. These types of optic fiber cables are ubiquitous and can be deployed at a lower cost compared to deploying expensive conventional geophones. In the oil and gas industry, DAS have been deployed in productions wells for vertical seismic profiling (VSP) applications to monitor oil reservoirs. Because the fiber can be cemented behind the borehole casing, there would be no need to stop production when collecting DAS data, thus saving a considerable amount of time and money. Another advantage of DAS data is that because data are measured continuously along space, DAS data have denser spatial coverage compared to an array of conventional geophones. The typical receiver spacing for a seismic survey is usually greater than 10 m while the spatial sampling of a DAS data can be around 1 m. However, a disadvantage of DAS data is that it has lower signal-to-noise ratio compared to geophone data.

---

* J. Ajo-Franklin, T. Baumgartner, K. Beckers, D. Blankenship, A. Bonneville, L. Boyd, S. Brown, J.A. Burghardt, C. Chai, Y. Chen, B. Chi, K. Condon, P.J. Cook, D. Crandall, P.F. Dobson, T. Doe, C.A. Doughty, D. Elsworth, J. Feldman, Z. Feng, A. Foris, L.P. Frash, Z. Frone, P. Fu, K. Gao, A. Ghassemi, Y. Guglielmi, B. Haimson, A. Hawkins, J. Heise, C. Hopp, M. Horn, R.N. Horne, J. Horner, M. Hu, H. Huang, L. Huang, K.J. Im, M. Ingraham, E. Jafarov, R.S. Jayne, S.E. Johnson, T.C. Johnson, B. Johnston, K. Kim, D.K. King, T. Kneafsey, H. Knox, J. Knox, D. Kumar, M. Lee, K. Li, Z. Li, M. Maceira, P. Mackey, N. Makedonska, E. Mattson, M.W. McClure, J. McLennan, C. Medler, R.J. Mellors, E. Metcalfe, J. Moore, C.E. Morency, J.P. Morris, T. Myers, S. Nakagawa, G. Neupane, G. Newman, A. Nieto, C.M. Oldenburg, T. Paronish, R. Pawar, P. Petrov, B. Pietzyk, R. Podgorney, Y. Polsky, J. Pope, S. Porse, J.C. Primo, C. Reimers, B.Q. Roberts, M. Robertson, W. Roggenthen, J. Rutqvist, D. Rynders, M. Schoenball, P. Schwering, V. Sesetty, C.S. Sherman, A. Singh, M.M. Smith, H. Sone, E.L. Sonnenthal, F.A. Soom, P. Sprinkle, C.E. Strickland, J. Su, D. Templeton, J.N. Thomle, V.R. Tribaldos, C. Ulrich, N. Uzunlar, A. Vachaparampil, C.A. Valladao, W. Vandermeer, G. Vandine, D. Vardiman, V.R. Vermeul, J.L. Wagoner, H.F. Wang, J. Weers, N. Welch, J. White, M.D. White, P. Winterfeld, T. Wood, S. Workman, H. Wu, Y.S. Wu, E.C. Yildirim, Y. Zhang, Y.Q. Zhang, Q. Zhou, M.D. Zoback

In this paper, we process and analyze DAS data collected at the first EGS Collab testbed for fracture characterization before, during, and after hydraulic stimulation. This testbed is located at 4850 ft. below the surface at the Sanford Underground Research Facility (SURF) in Leads, South Dakota. This testbed consists of one production well (E1-P), one injection well (E1-I) and six monitoring wells around a fracture stimulation zone. Four of these monitoring wells (E1-PST, E1-PSB, E1-PDT, and E1-PDB) are parallel to the created fractures and two of these wells (E1-OT and E1-OB) are orthogonal to the fractures. Each of the monitoring wells are about 60 m in depth. We show a diagram representing the geometry of the test site in Figure 1. The DAS fiber was deployed in these six monitoring wells. We use the sources from a multi-level continuous active-seismic source monitoring (ML-CASSM) system (Ajo-Franklin et al. 2011; Daley et al. 2011, Gao et al. 2018; Pan et al. 2019; Chi et al. 2019) as the source for this experiment. CASSM is an array of automated multilevel sources and receivers permanently installed in the wells. We compare the DAS data with the CASSM data.

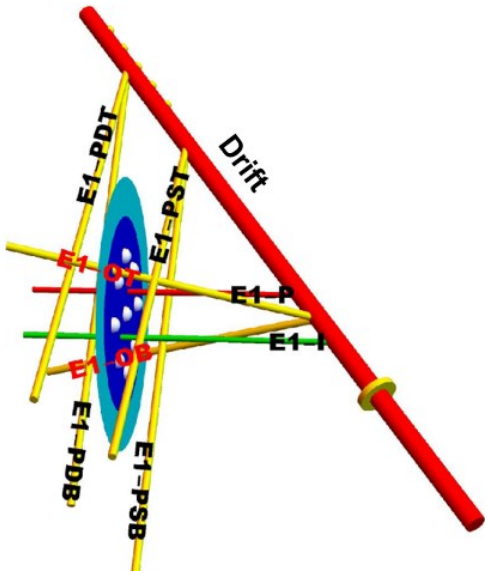

Figure 1. 3D Map view of the EGS Collab test site. The thick red line represents the drift (tunnel). The red thin red line represents the production well (E1-P). The green line represents the injection well (E1-I). The yellow lines represent the six monitoring wells. The green and blue circle represents the fracture zone. Two monitoring wells (E1-OT and E1-OB) are orthogonal to the fracture zone and four monitoring wells (E1-PDT, E1-PDB, E1-PST, and E1-PSB) are parallel to the fracture zone. Modified from (Huang et al. 2017).

2. DATA ACQUISITION

For the survey, we use one continuous fiber cable approximately 1600 m in length to collect the DAS data. The fiber was deployed in the six monitoring wells around the stimulation and production wells. The fiber is looped in and out of each monitoring well to record the DAS data. The fiber in-between the monitoring wells is left free hanging in the drift. The end of the fiber is attached to a Silixa iDAS interrogator unit, which records the DAS data. The channel spacing is set to 1 m and the gauge length is set to 10 m. DAS data was collected continuously from April 5, 2018 to June 26, 2018. For most of the recording history, the DAS data was acquired with a 1 kHz sampling frequency. However, we use a 10 kHz sampling frequency during and around hydraulic stimulation (May 22, 2018 – May 25, 2018). In total, five stimulations were conducted from May 22-25 (Fu et al. 2018).

We use CASSM sources as the sources for our DAS data. The CASSM observation system is an array of automated sources and receivers permanently installed in the monitoring wells. The CASSM array contains a total of 17 CASSM sources, 24 hydrophones, and 18 accelerometer receivers deployed in the six monitoring wells. The 17 CASSM sources are deployed across four of the monitoring wells: six sources in E1-PST, five sources in E1-PSB, five sources in E1-OB, and one source in E1-PDT. The 24 hydrophones were deployed in two wells: E1-OT and E1-PDB. The 18 accelerometer receivers were deployed evenly across the six wells, three in each well. We show the geometry of the CASSM acquisition system in Figure 2. During data acquisition, each CASSM source emitted seismic waves that propagated into the surrounding media and arrived at the receiver arrays that recorded the signals. The DAS fiber deployed in the six monitoring wells also recorded the CASSM source signals. At each shot point, the CASSM source repeatedly fired 16 times. As a result, each common-shot gather of the CASSM data is a stack of 16 shots. Each of the CASSM sources went off in 10 minute intervals continuously over the course of the data acquisition period.

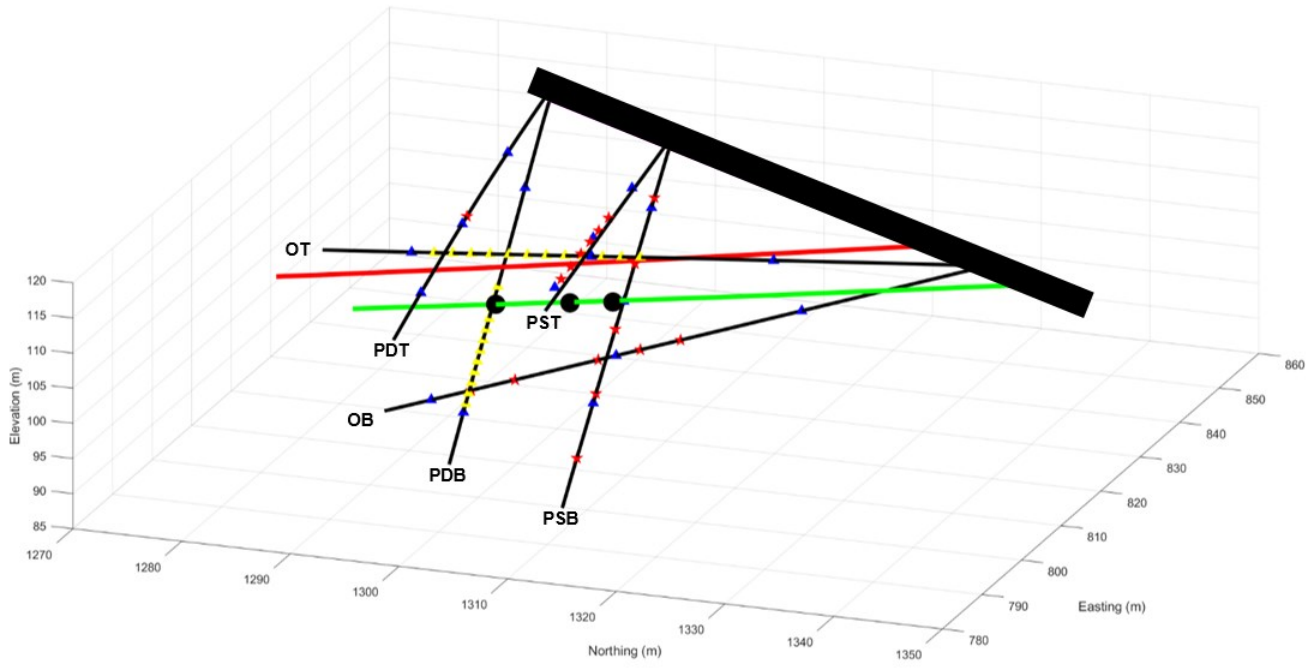

Figure 2. Geometry of the ML-CASSM acquisition system at the first EGS Collab testbed. The thick black line is the drift. The red line represents the production well. The green line represents the injection well. The thin black lines represent the six monitoring wells. The red stars indicate the 17 CASSM sources. The yellow triangles indicate the 24 hydrophones. The blue triangles indicate the 18 accelerometers. The black circles represent the notch positions cut in the injection well. The DAS fiber is deployed in the six monitoring wells.

3. PROCESSING DAS DATA AND PRELIMINARY RESULTS

We show an example of one second of the raw 10 kHz DAS data collected by all channels of the fiber in Figure 3. As can be seen in the figure, the data appears very noisy and we cannot distinguish any coherent signals. To compare with the CASSM data, we first remove the water level in the data by subtracting a moving window average from the raw strain-rate DAS data. We then integrate the stain-rate data over time to obtain strain, and apply band-pass filtering and median filtering to the data to remove additional noise.

The common-shot record of the CASSM data is a stack of 16 shots from the CASSM source. Since the DAS data were acquired continuously, we must find the time at which the CASSM source was fired on the DAS data trace. We first extract the DAS data that corresponds to the location of a source in the well. We find the spike in the data that corresponds to 16 shots from the CASSM source. We pick the time of the spikes and select a window around that picked time and stack them together to obtain DAS data comparable to the CASSM data. We show a single trace with 16 spikes on the trace showing the time at which the CASSM shots were fired along with the stacked trace of the 16 shots and a time shifted CASSM trace in Figure 4. In the following we show data collected in wells OB and OT on different days. We show stacked data of data recorded in wells OB and OT on May 23, 2018 at 12:38:55 UTC in Figure 5, the stacked data recorded in wells OB and OT on May 24, 2018 at 12:36:55 UTC in Figure 6, and the stacked data recorded in wells OB and OT on May 25, 2018 at 12:36:06 UTC in Figure 7. On all three figures, we can easily distinguish the strong signal corresponding to the source. This strong signal occurs both in the area of the fiber that is going down the borehole and coming back up the borehole. However, we note that this signal does not seem to transmit to other parts of the fiber. We may need to use a smaller gauge length when recording the data to record this signal.

We also compare data before and after stimulation to see if there is any scattering caused by stimulation. The first major stimulation that occurred was the third stimulation on 5/24/2018 at approximately 22:38:00. We plot data for two wells approximately 10 minutes before stimulation, 10 minutes after the starting stimulation, and the difference between the two data sets in Figure 1Figure 8. From the figure we see that the data has higher energy during stimulation. However, we still do not see any coherent events in either the recorded data or the difference data.

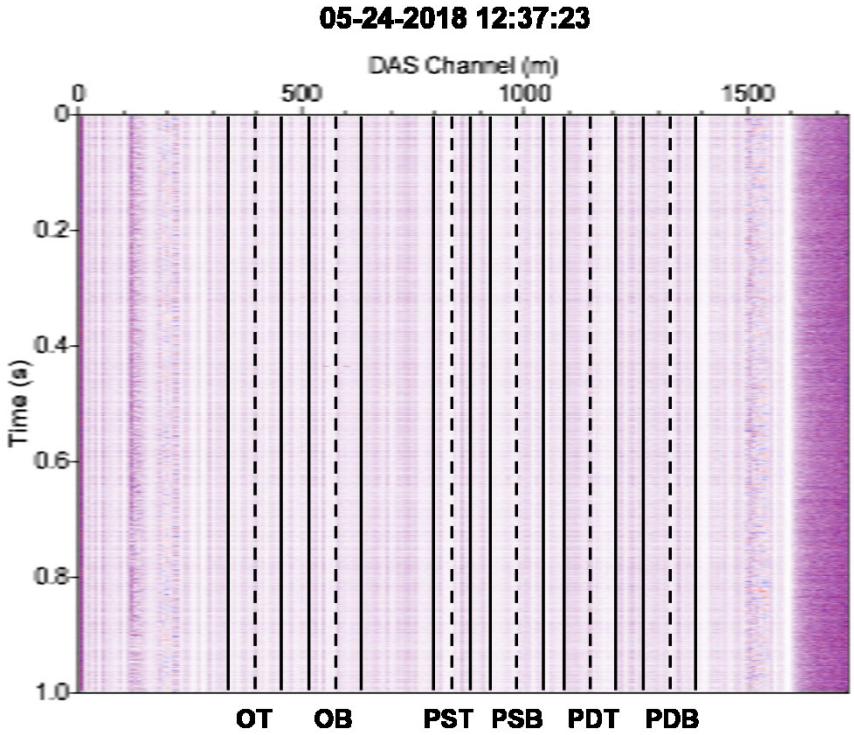

Figure 3. Example of 1 second of the 10 kHz DAS data. The solid black vertical lines show the channel on the data that correspond to where the fiber enters and exits each well. The black line represents the channel corresponding to the bottom of each well. For each well, the fiber enters the top of the well, goes down to the bottom, bends, then comes back up the well and exits the well.

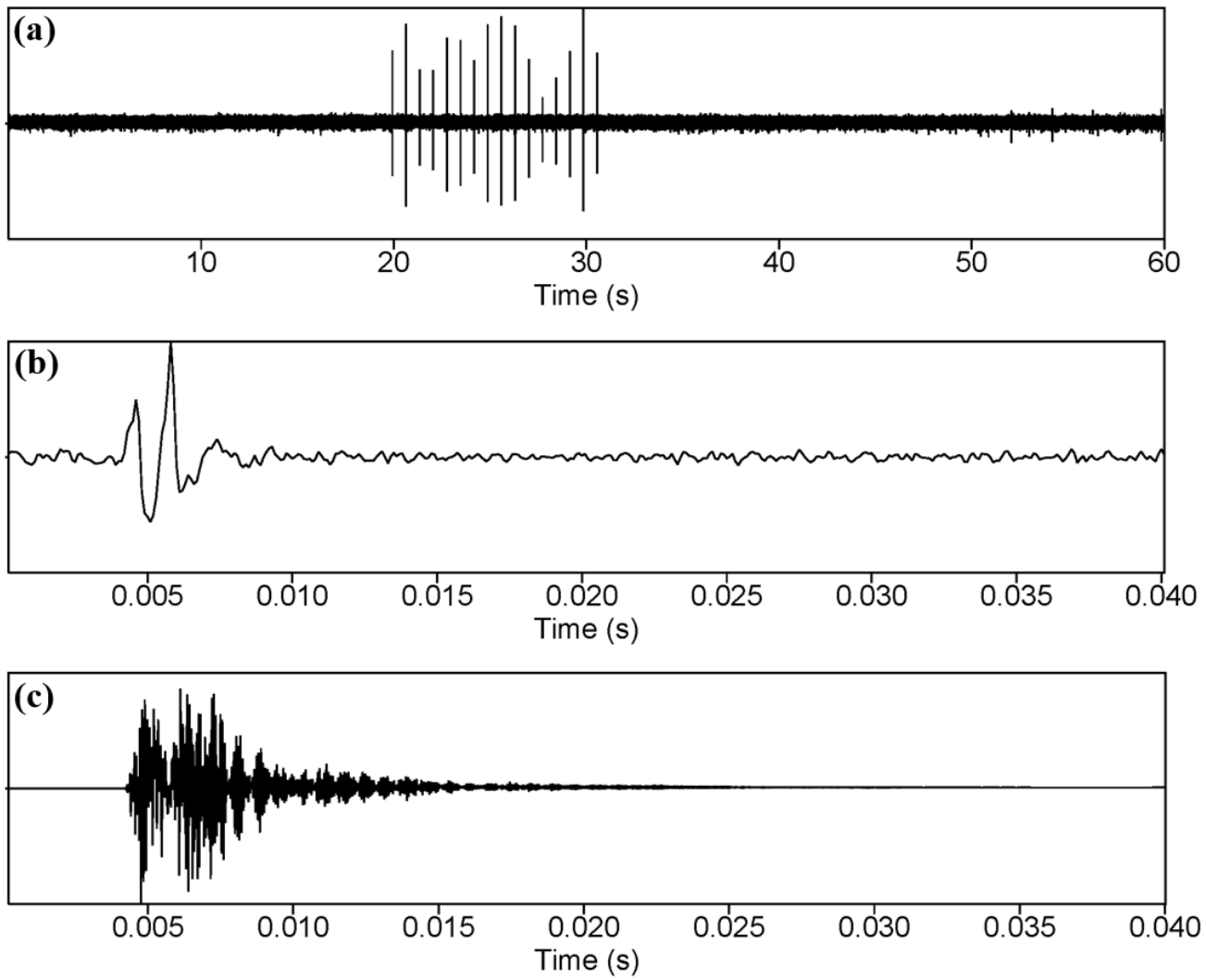

Figure 4. (a) A 60 second long trace extracted from Channel 602 from data collected starting on 05/24/2018 12:36:55 UTC. This channel corresponds to a depth of 34 m in well OB where a CASSM source was collected at that time. The 16 impulses between 20-30 s correspond to the CASSM source taking shots. (b) The stack of all 16 source events to form a single trace. (c) Time shifted trace of the CASSM data from an accelerometer in OB.

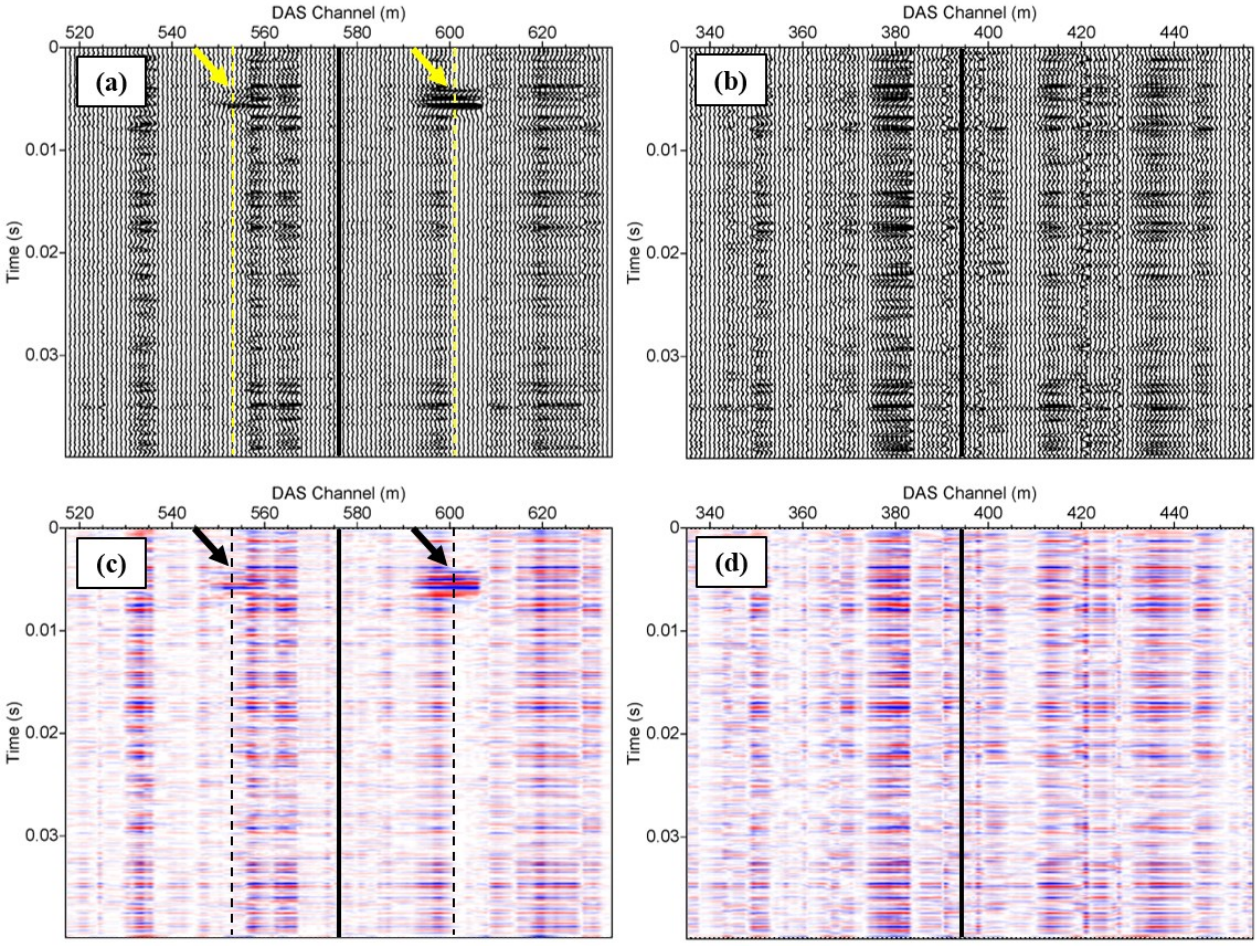

Figure 5. DAS data collected on May 23, 2018 at 12:36:09 UTC (a) Wiggle plot of DAS data collected in well OB. (b) Wiggle plot of DAS data collected from well OT. (c) Variable density plot of DAS data collected in well OB. (d) Variable density plot of DAS data collected in well OT. The CASSM source is located at depth of 34 m in well OB. The dashed lines indicate the depth of the source on the data plot. The arrows point to the source signal in the data. This signal is very strong and located in the correct position in the data. The black line dividing the data horizontally is the bottom of the well. The fiber goes into the well, bends at the bottom, then comes back up. We however, cannot distinguish any other coherent events other than the source signal. This signal also does not seem to transmit to far offsets.

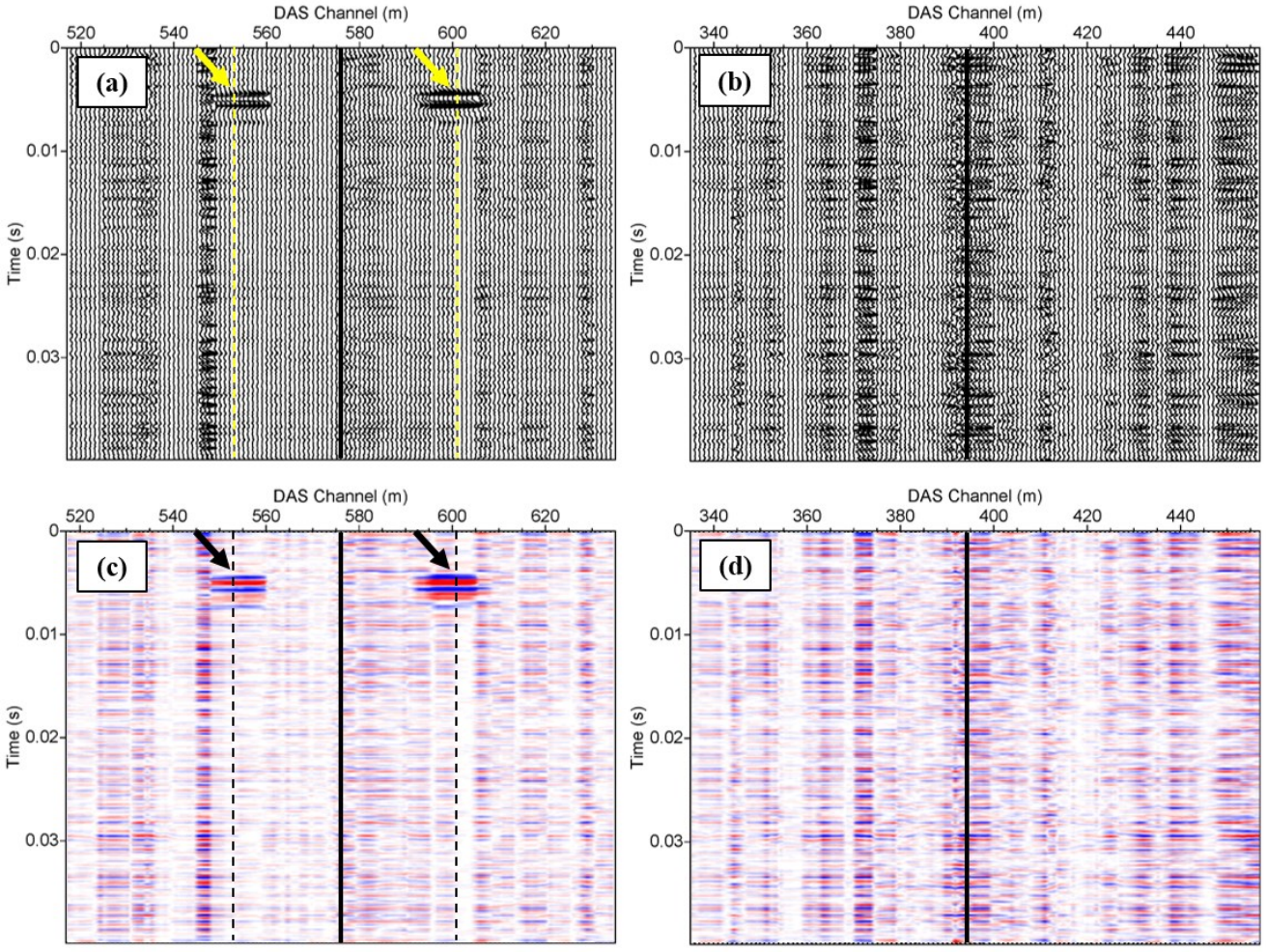

Figure 6. DAS data collected on May 24, 2018 at 12:36:55 UTC (a) Wiggle plot of DAS data collected in well OB. (b) Wiggle plot of DAS data collected from well OT. (c) Variable density plot of DAS data collected in well OB. (d) Variable density plot of DAS data collected in well OT. The CASSM source is located at depth of 34 m in well OB. The dashed lines indicate the depth of the source on the data plot. The arrows point to the source signal in the data. This signal is very strong and located in the correct position in the data. The black line dividing the data horizontally is the bottom of the well. The fiber goes into the well, bends at the bottom, then comes back up. We however, cannot distinguish any other coherent events other than the source signal. This signal also does not seem to transmit to far offsets.

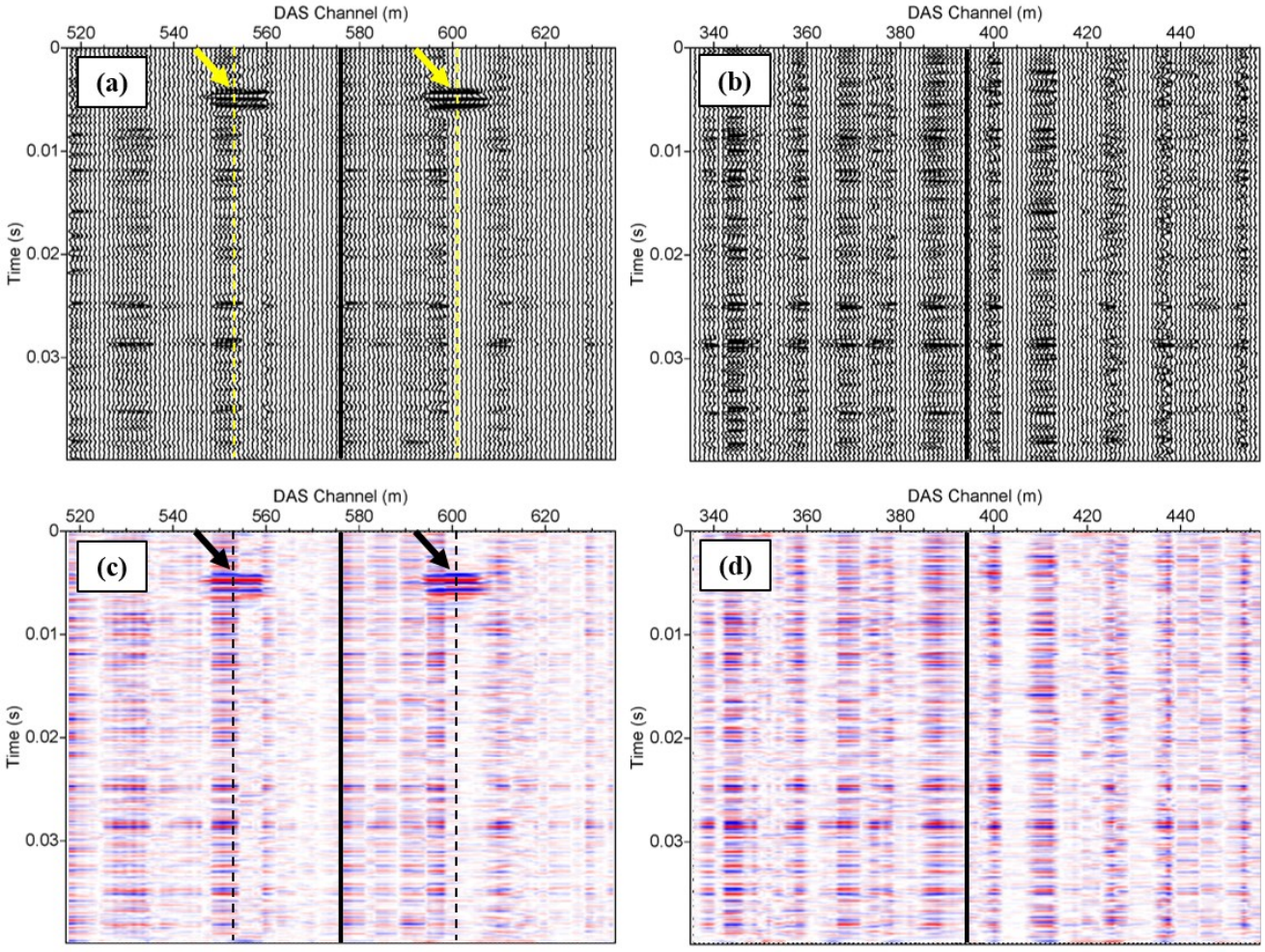

Figure 7. DAS data collected on May 25, 2018 at 12:36:09 UTC (a) Wiggle plot of DAS data collected in well OB. (b) Wiggle plot of DAS data collected from well OT. (c) Variable density plot of DAS data collected in well OB. (d) Variable density plot of DAS data collected in well OT. The CASSM source is located at depth of 34 m in well OB. The dashed lines indicate the depth of the source on the data plot. The arrows point to the source signal in the data. This signal is very strong and located in the correct position in the data. The black line dividing the data horizontally is the bottom of the well. The fiber goes into the well, bends at the bottom, then comes back up. We however, cannot distinguish any other coherent events other than the source signal. This signal also does not seem to transmit to far offsets.

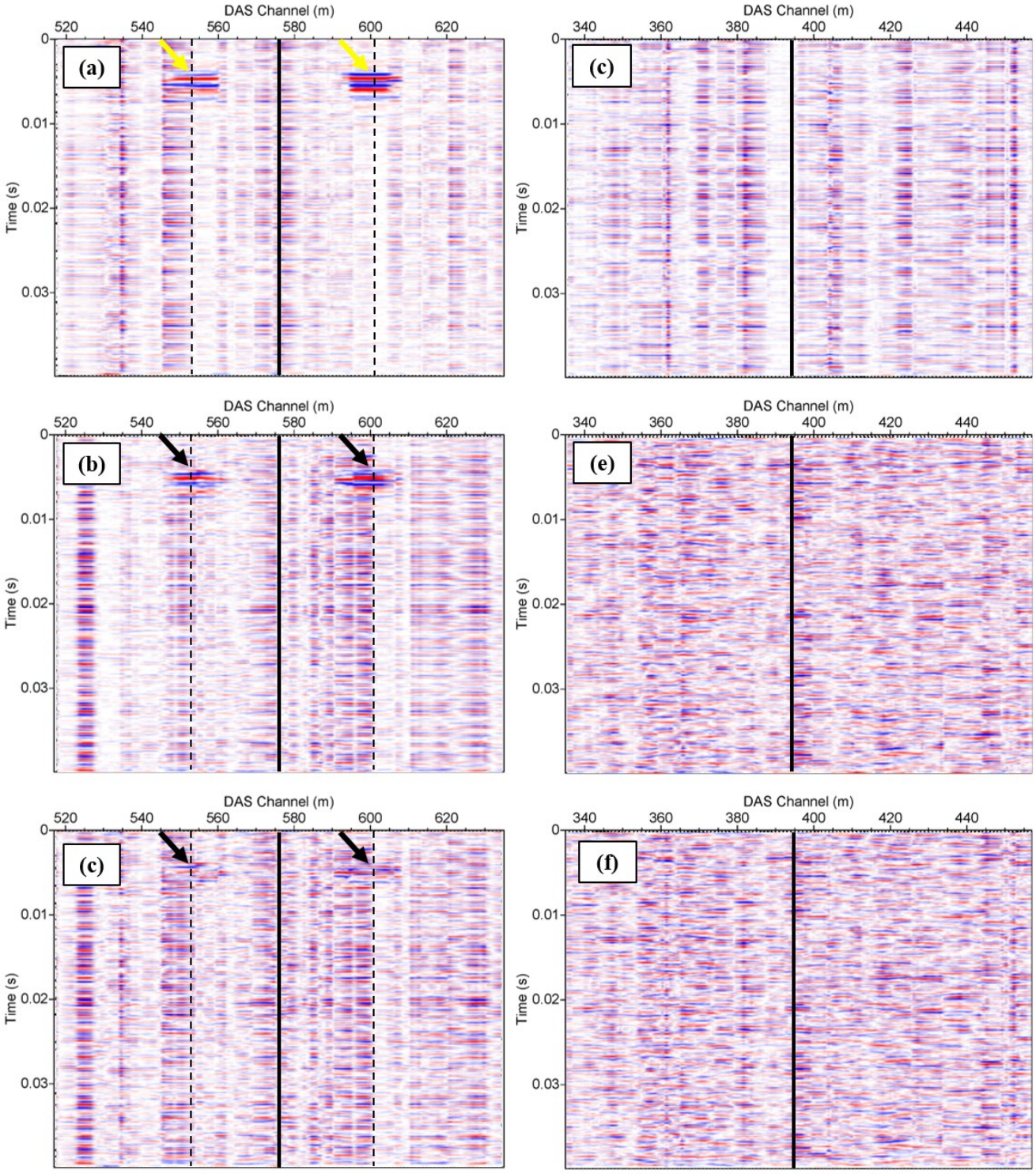

Figure 8. (a) Data from well OB recorded on 5/24/2018 22:29:39, approximately 10 minutes before the start of the third stimulation. (b) Data from well OB recorded at 5/24/2018 22:48:09 approximately 10 minutes after the start of the third stimulation. (c) The difference between (b) and (a). (d) Data from well OT recorded on 5/24/2018 22:29:39, approximately 10 minutes before the start of the third stimulation. (e) Data from well OT recorded at 5/24/2018 22:48:09 approximately 10 minutes after the start of the third stimulation. (f) The difference between (e) and (d). The solid black line represents the bottom of the well where the fiber bends. The dashed lines and the arrows indicated the depth of the CASSM source.

CONCLUSIONS

We have analyzed and processed the 10 kHz DAS data acquired at the EGS Collab sight and obtained preliminary results. We picked the times on the continuous DAS data corresponding to the CASSM source times and stacked the data to obtain comparable data to CASSM data. We show preliminary results for several shots across three days. We find the CASSM source signature is obvious on the DAS data for channels in the same monitoring well as where the source is located. However this source signature is only found around 10 m near the source location and disappears at greater offsets from the source. We do not find any signal in any other of the monitoring wells in which the CASSM sources were not placed. We also compared data before and after stimulation. We subtracted the data before and after stimulation. However, we were still unable to obtain any coherent signals in our preliminary results. The lack of coherent signals in the DAS data from CASSM might be caused by the 10 m gauge length used to acquire this DAS dataset.

ACKNOWLEDGEMENTS

This material was based upon work supported by the U.S. Department of Energy (DOE), Office of Energy Efficiency and Renewable Energy (EERE), Office of Technology Development, Geothermal Technologies Office, under Contract No. 89233218CNA000001 to Los Alamos National Laboratory (LANL). LANL is operated by Triad National Security, LLC, for the National Nuclear Security Administration (NNSA) of U.S. DOE. The United States Government retains, and the publisher, by accepting the article for publication, acknowledges that the United States Government retains a non-exclusive, paid-up, irrevocable, world-wide license to publish or reproduce the published form of this manuscript, or allow others to do so, for United States Government purposes. The research supporting this work took place in whole or in part at the Sanford Underground Research Facility in Lead, South Dakota. The assistance of the Sanford Underground Research Facility and its personnel in providing physical access and general logistical and technical support is acknowledged. We thank Dr. Yingping Li for insightful discussions.

REFERENCES

Ajo-Franklin, J.B., Daley, T.M., Butler-Veytia, B., Peterson, J., Wu, Y., Kelley, B., and Hubbard, S.: Multi-level continuous active source seismic monitoring (ML-CASSM): Mapping shallow hydrofracture evolution at a TCE contaminated site, *Extended Abstracts of Society of Exploration Geophysicists Annual Meeting*, (2011).

Ajo- Franklin, J. B., Dou, S., Lindsey, N. J., Monga, I., Tracy, C., Robertson, M., Tribaldos, V. R., Ulrich, C., Freifeld, B., Daley, T., & Li, X.: Distributed acoustic sensing using dark fiber for near-surface characterization and broadband seismic event detection, Scientific Reports, **9**, (2019).

Chi, B., Huang, L., Gao, K., Ajo-Franklin, J., Kneafsey, T.J., and EGS Collab Team: High-resolution imaging of created fractures in EGS Collab experiment Using CASSM data, *GRC Transactions*, **43**, (2019).

Daley, T., Ajo-Franklin, J.B., and Doughty, C.: Constraining the reservoir model of an injected CO2 plume with crosswell ML-CASSM at the Frio-II Brine Pilot, *International Journal of Greenhouse Gas Control*, **5**, 2, (2011), 1022-1030.

Daley, T.M., Miller, D.E., Dodds, K., Cook, P., and Freifeld, B.M.: Field testing of modular borehole monitoring with simultaneous distributed acoustic sensing and geophone vertical seismic profiles at Citronelle, Alabama, *Geophysical Prospecting*, **64**, (2016), 1318-1334.

Fu, P., M. White, J. Morris, T. Kneafsey, and E.C. Team: Predicting Hydraulic Fracture Trajectory under the Influence of a Mine Drift in EGS Collab Experiment I, in PROCEEDINGS, 44th Workshop on Geothermal Reservoir Engineering, edited, Stanford University, Stanford, California, (2018).

Gao, K., Huang, L., Chi, B., Ajo-Franklin, J., and the EGS Collab Team: Imaging fracture zones using continuous active source seismic monitoring for the EGS Collab Project: a synthetic study, *Proceedings*, 43rd Workshop on Geothermal Reservoir Engineering, Stanford University, Stanford, CA (2018).

Huang, L., Chen, Y., Gao, K., Fu,, P., Morris, J., Ajo-Franklin, J., Nakagawa, S., and EGS Collab Team: Numerical modeling of seismic and displacement-based monitoring for the EGS Collab Project, *GRC Transactions*, **41**, (2017).

Jousset, P., Reinsch T., Ryberg, T., Blanck, H., Clarke, A., Aghayev, R., Hersir, G.P., Henninges, J., Weber, M., and Krawczyk, C.M.: Dynamic strain rate determination using fibre-optic cables allows imaging of seismological and structural features, *Nature Communications*, **9:2509**, (2018).

Karrenbach, M., Cole, S., Ridge, A., Boone, K., Kahn, D., Rich, J., Silver K., Langton, D.: Fiber-optic distributed acoustic sensing of microseismicity, strain and temperature during hydraulic fracturing, *Geophysics*, **84**, (2019), D11-D23

Martin, E.R, Lindsey, N.J., Dou, S., Ajo-Franklin, J.B., Wagner, A., Bjella, K., Daley, T.M., Freifeld, B., Robertson, M., Ulrich, C.: Interfermetry of a roadside DAS array in Fairbanks, AK, *Extended Abstracts of Society of Exploration Geophysicists Annual Meeting*, (2016).

Mateeva, A., Lopez, J., Mestayer, J., Willis, P., Cox, B., Kiyashchenko, D., Yang, Z., Berlang, W., Detomo, R., and Grandi, S.: Distributed acoustic sensing for reservoir monitoring with VSP, *The Leading Edge*, (2013).

Mateeva, A., Lobez, Potters, H., Mestayer, J., Cox, B., Kiyashchenko, D., Wills, P., Grandi, S., Hornman, K., Kuvshinov, B., Berlang, W., Yang, Z., and Detomo, R.: Distributed acoustic sensing for reservoir monitoring with vertical seismic profiling, *Geophysical Prospecting*, **62**, (2014), 679-692.

Mestayer, J., Cox, B., Wills, P., Kiyashchenko, D., Lopez, J., Costello, M., Bourne, S., Ugueto, G., Lupton, R., and, Solano, G.: Field trials of distributed acoustic sensing for geophysical monitoring, *Extended Abstracts of Society of Exploration Geophysicists Annual Meeting*, (2011).

Molenaar, M.M., Hill, D.J., Webster, P., Fidan, E., and Birch, B., First downhole application of distributed acoustic sensing for hydraulic-fracturing monitoring and diagnostics, *SPE Drilling and Completion*, (2012)

Pan, W., Huang, L., Gao, K., Ajo-Franklin, J., Kneafsey, T.J., and EGS Collab Team: Anisotropic elastic-waveform inversion and least-squares reverse-time migration of CASSM data for experiment I of the EGS Collab Project, *Proceedings*, 43rd Workshop on Geothermal Reservoir Engineering, Stanford University, Stanford, CA (2018).

Poletto, F., Finfer, D., Corubolo, P., and Farina, B.: Dual wavefields from distributed acoustic sensing measurements, *Geophysics*, **81**, (2016), D585-D597.

Zhu, T., and Stensrud, D.J.: Characterizing thunder-induced ground motion using fiber-optic distributed acoustic sensing array, Joural of Geophysical Research: Atmospheres, 124, (2019), 12.810-12.823.